Chapter 8: Scanning Electrochemical Microscopy of DNA Monolayers Modified with Nile Blue

Adapted from: Gorodetsky, A. A., Hammond, W., Hill, M. G., Slowinski, K., Barton, J. K. (2008) *Langmuir ASAP*.

Electrochemical measurements were performed in collaboration with William Hammond.

ABSTRACT

Scanning electrochemical microscopy (SECM) is used to probe long range charge transport (CT) through DNA monolayers containing the redox-active Nile Blue (NB) intercalator covalently affixed at a specific location in the DNA film. At substrate potentials negative of the formal potential of covalently attached NB, the electrocatalytic reduction of $Fe(CN)_6^{3-}$ generated at the SECM tip is observed only when NB is located at the DNA/solution interface; for DNA films containing NB in close proximity to the DNA/electrode interface, the electrocatalytic effect is absent. This behavior is consistent with both rapid DNA-mediated CT between the NB intercalator and the gold electrode as well as a rate-limiting electron transfer between NB and the solution phase $Fe(CN)_6^{3-}$. The DNA-mediated nature of the catalytic cycle is confirmed through sequence-specific and localized detection of attomoles of TATA-binding protein, a transcription factor which severely distorts DNA upon binding. Importantly, the strategy outlined here is general and allows for the local investigation of the surface characteristics of DNA monolayers both in the absence and presence of DNA-binding proteins. These experiments highlight the utility of DNA-modified electrodes as versatile platforms for SECM detection schemes that take advantage of CT mediated by the DNA base-pair stack.

8.1 Introduction

Numerous studies have shown that DNA efficiently mediates long range charge transport both in solution (1–5) and at DNA-modified surfaces (6–7). The electrochemical response at DNA self-assembled monolayers (SAMs) is remarkably sensitive to base stacking perturbations, with the efficiency of CT to an electroactive probe reflecting the integrity of the base pair stack. Consequently, DNA electrochemistry has been exploited successfully in the development of simple assays for the rapid detection of single-nucleotide polymorphisms (8–10), base lesions (11), and DNA/protein binding (12–18).

Controlling the orientation and packing of DNA helices within these SAMs is critical for many analytical applications, yet assessing film morphology and homogeneity, particularly in aqueous media, remains a difficult challenge. Previously, the morphology of DNA SAMs on gold has been investigated by scanning tunneling microscopy (STM) (19–21), atomic force microscopy (AFM) (22–24), and most recently, scanning electrochemical microscopy (SECM) (25–28). SECM provides submicron visualization of DNA films through *in situ* imaging of chemical reactivity at modified insulating or conducting substrates (29, 30). SECM is also inherently compatible with aqueous environments, thereby allowing for the direct electrochemical profiling of DNA arrays with micron resolution (29, 30). In addition, SECM has been used successfully to monitor DNA hybridization and to detect DNA lesions (29–34). One advantage of this technique over conventional bulk electrochemistry is that the micron-level diameter of the SECM

tip inherently minimizes contributions from imperfections on large-sized electrodes by sampling a local area of the film at a specific substrate potential.

Electrochemical assays based on DNA CT have frequently utilized non-covalent mediators to collect global information (8–11, 35, 36), but the electrochemistry of these mediators can be significantly complicated by contributions from CT pathways that are not DNA-mediated (37). The use of covalent probes at fixed positions within the film (38–45), particularly in conjunction with backfilling of the DNA monolayer with a suitable straight-chain diluent molecule, minimizes such contributions from defects, pinholes, and other imperfections. Therefore, SECM investigations of DNA monolayers can particularly benefit from the use of covalently attached probes.

Here, we report the application of SECM in probing long range CT across a DNA monolayer containing the redox-active intercalator Nile Blue (NB) covalently attached at discrete sites along the individual DNA helices. Nile Blue is particularly useful for such studies since it can be easily incorporated into DNA on solid support and displays catalytic activity (13). Therefore, based on our previous investigations of the catalytic reduction of ferricyanide by methylene blue (MB) at DNA-modified electrodes (8–11, 46), we have replaced MB with covalently bound NB to reduce ferricyanide, which is generated at the SECM tip in our current experiments. Only Nile Blue attached at the solution-exposed periphery of the film is capable of supporting catalytic regeneration of ferrocyanide present in solution. Furthermore, this cycle can be interrupted in a sequence-specific manner by addition of TATA Binding Protein (TBP), a transcription factor that bends DNA by ~ 90º upon binding (12, 13). Taken together, these studies establish the upright orientation of individual helices within a relatively homogeneous dilute

monolayer and demonstrate the critical role of efficient long-range electrochemical charge transport through the π-stack. They additionally suggest a sensitive and highly selective SECM method for assaying specific DNA/protein interactions with even dilute and imperfect assemblies of probe DNA.

8.2 Experimental

8.2.1 Materials

All reagents for DNA synthesis were purchased from Glen Research. Methylene blue, ruthenium hexammine chloride, potassium ferricyanide, potassium ferrocyanide, and 11-mercaptoundecylphosphoric acid were purchased from Sigma in the highest purity available and used as received. Nile Blue perchlorate was purchased from Acros in laser grade purity. TATA Binding protein was custom ordered from Protein One, Inc. Bovine Serum Albumin (BSA) was obtained from New England Biolabs, Inc. Platinum scanning electrochemical microscopy tips were purchased from CH Instruments, Inc. as used as received. Au (111) on mica substrates packaged under argon were purchased from Agilent, Inc., and utilized immediately. Sodium phosphate buffers were prepared with Milli-Q water and pH adjustments were made with sodium hydroxide, if necessary.

8.2.2 Synthesis of Thiol and Nile Blue-Modified DNA

Oligonucleotides were prepared on solid support using standard phosphoramidite chemistry on an Applied Biosystems 394 DNA synthesizer. All of the prepared sequences were purified by multiple rounds of reverse-phased, high-performance liquid chromatography (HPLC). The pure oligonucleotides were characterized with matrix-

assisted laser desorption (MALDI) mass spectrometry and UV-visible (UV-Vis) spectrophotometry.

Thiol-terminated oligonucleotides were synthesized according to established protocols from Glen Research, Inc. using the C6 S-S thiol modifier. After deprotection and cleavage from solid support with ammonium hydroxide (60 ºC for 8 hours), the disulfide containing DNA was purified by HPLC. The disulfide was subsequently reduced with an excess of dithiothreitol in ammonium acetate buffer at pH=8, and the free thiol containing single-stranded DNA was then purified with a second round of HPLC.

As schematically illustrated in Figure 8.1, DNA modified with NB at the 5' terminus was prepared according to ultra-mild protocols (Glen Research, Inc.) to avoid degradation of the NB moiety. Additionally, Pac-protected bases and ultra mild reagents were utilized during the synthesis to prevent undesirable capping of the protecting groups. A 17-mer sequence (either 5'-UGC GTG CTT TAT ATC TC-3' or 5'-UGC GCG CCC GGC GCC TC-3') was prepared on solid support with a 5-[3-acrylate NHS Ester]-deoxy uridine as the terminal 5' base. The beads were then removed from the synthesizer and dried thoroughly. The solid support were reacted with a 10 mg/mL Nile Blue perchlorate solution in either 9:1 N,N-dimethylformamide/N,N-diisopropylethylamine or 9:1 dichloromethane/N,N-diisopropylethylamine for 12–48 hours. The beads were subsequently washed up to three times with dichloromethane or N,N-dimethylformamide, methanol, and acetonitrile. Subsequently, the Nile Blue-containing sequence was simultaneously cleaved from the support and deprotected with 0.05 M potassium

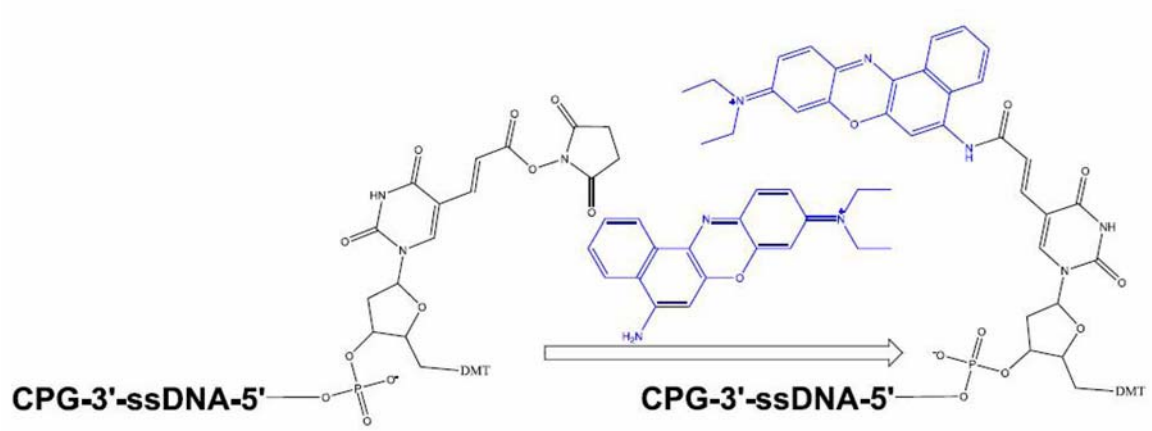

Figure 8.1: Schematic illustration of the coupling of Nile Blue to the NHS-Carboxy-dT modified DNA on solid support (CPG)

carbonate in methanol at room temperature for 12–14 hours. The overall yields of the reaction ranged from 30% to 80%.

DNA modified with NB one base in from the 3' terminus was prepared according to ultra-mild protocols in a similar fashion. A 2-mer sequence containing a 5-[3-acrylate NHS Ester]-deoxy uridine as the terminal 5' base was prepared on solid support. The beads were removed from the synthesizer and reacted with a 10 mg/mL Nile Blue perchlorate solution in either 9:1 N,N-dimethylformamide/N,N-diisopropylethylamine or 9:1 dichloromethane/N,N-diisopropylethylamine for 12–48 hours. After thorough washing of the beads, the Nile Blue containing 2-mer was placed back on the synthesizer and the remaning 15 bases were added to the sequence, yielding the oligonucleotide 5'-TGC GTG CTT TAT ATC UC-3'. The resulting sequence contained an internal Nile Blue and was deprotected with 0.05 M potassium carbonate in methanol at room temperature for 12-14 hours. The overall yields of the reaction ranged from 30% to 80%.

Both thiol- and NB-modified DNA was quantified using the extinction coefficient of the single-stranded DNA at 260 nm on a Beckman UV-Vis spectrophotometer. Equimolar amounts of each strand (50 μM) were combined before the resulting solution was purged with argon. Duplexes were formed by thermally annealing in deoxygenated buffer containing 5 mM NaP_i, pH = 7.1, 50 mM NaCl to 90 ºC, followed by cooling to ambient temperature.

8.2.3 Preparation of Backfilled DNA/11-mercaptoundecylphosphoric Acid Monolayers

Electrode areas were defined with a Viton o-ring with estimated surface areas of either 0.1 cm^2 or 0.2 cm^2 in either a scanning electrochemical microscope teflon cell from

CH Instruments, Inc., or a custom-built teflon cell. To ensure successful experiments, great care was taken to minimize mechanical damage to the gold substrate upon mounting in the cell. After cell assembly, a fresh 25–50 μM duplex NB-DNA solution was deposited onto the gold surface. Monolayer formation was allowed to proceed in a humidified environment for a period of 24–72 hours. Incubation times outside of this window (either shorter or longer) were found to be detrimental to proper monolayer formation. Upon completion of film formation, the cell was rinsed thoroughly with phosphate buffer to remove residual DNA before the DNA-modified surface was backfilled with 11-mercaptoundecylphosphoric acid for 10–20 minutes (47). Mercaptoundecylphosphoric acid rapidly displaces DNA from the surface, so backfilling times were short and the cell was rinsed thoroughly to eliminate any residual alkanethiols.

8.2.4 Electrochemistry/Scanning Electrochemical Microscopy Experiments

Cyclic voltammetry and scanning electrochemical microscopy experiments were performed using a CH Instruments electrochemical analyzer (Austin, TX). Unless otherwise noted, experiments were performed at ambient temperature in phosphate buffer at pH 7 containing either 5 mM NaP_i and 50 mM NaCl or 20 mM NaP_i and 80 mM NaCl under an Argon atmosphere (the oxygen content was constantly monitored). The buffer was supplemented with $K_4Fe(CN)_6$ for SECM experiments. A teflon electrochemical cell was used for all experiments with a Pt auxiliary electrode, a gold working electrode, and a silver/silver chloride (Ag/AgCl) reference electrode. Since we have observed some variation in the potential of covalently attached NB depending on the type of gold surface and the buffer conditions, the voltammetric potentials reported in this work have a maximum uncertainty of 50 mV.

In a typical SECM experiment, total or partial passivation of the substrate was confirmed through cyclic voltammetry of the ferri/ferrocyanide couple at the substrate. Approach curves were obtained with either 2 μm or 10 μm diameter platinum tips which were polarized between 600 mV and 1 V, and identical results were obtained regardless of the tip bias. To aid interpretation of the results, substrates featuring a significant free NB signal or virtually no passivation against ferricyanide were discarded. Initial approach curves to the substrate were recorded at a 0 mV substrate bias to confirm the insulating behavior of the NB-DNA monolayer. Subsequent approach curves were recorded with the substrate bias modulated between 0 mV and -400 mV. For imaging of the substrate, the SECM tip was moved to within less than one tip radius of the substrate before being retracted by 2–5 microns prior to scans. Great care was taken during all experiments to avoid damaging the DNA monolayer through direct contact of the tip with the surface.

8.2.5 TATA Binding Protein Experiments

In a typical TBP detection experiment by SECM, approach curves or substrate scans were initially recorded with the bias modulated between 0 mV and -400 mV to confirm switching from negative to positive feedback. Subsequently, TBP was added to the SECM cell from a concentrated ~16 μM stock in phosphate buffer at pH = 7 containing 5 mM KP_i, 50 mM NaCl, 4 mM $MgCl_2$, 4 mM spermidine, 50 μM EDTA, 10% glycerol. The solution was equilibrated via gentle pipetting, and approach curves or substrate scans were again recorded with the bias modulated between 0 mV and -400 mV.

8.3 Results

8.3.1 Electrochemistry of Backfilled DNA Monolayers Modified with Nile Blue

Figure 8.2 shows a schematic illustration of DNA monolayers modified with NB either at the top or bottom (Figure 8.1 shows the structure of the nucleotide). DNA monolayers modified with NB display a pH dependent redox couple at ~ -200 mV versus Ag/AgCl due to the 2e- reduction of the bound probe (13, 48, 49). Since modification of the exocyclic amine of NB perturbs its aromatic core with an accompanying shift in its redox potential of ~ 200 mV relative to free NB (50, 51), DNA monolayer stability can be assessed *in situ* with the appearance of a NB signal at ~ -400 mV indicating film degradation. Coulometric measurements of the NB signals for monolayers labeled at either the top or bottom yield typical DNA surface coverages of ~1–3 pmol/cm^2 (compared to ~ 40 pmol/cm^2 or greater for densely packed monolayers) (10). As expected for a surface-bound species, plots of peak current as a function of scan rate are linear, and the ratios of the cathodic to anodic charge are approximately unity (Figure 8.3) (52). Overall, the electrochemical characteristics of the two types of monolayers (functionalized at either the top or the bottom) are very similar, despite the ~ 45 Å difference in gold/NB separations. This observation is consistent with previous studies involving site-specific labeling of DNA monolayers with redox-active intercalators (13, 39, 40).

Based on previous work involving electrocatalytic reduction of ferricyanide at DNA-modified substrates via intercalated Methylene Blue (MB) (8, 46), we explored the electrochemistry of covalently bound NB in the presence of ferricyanide (Figure 8.4).

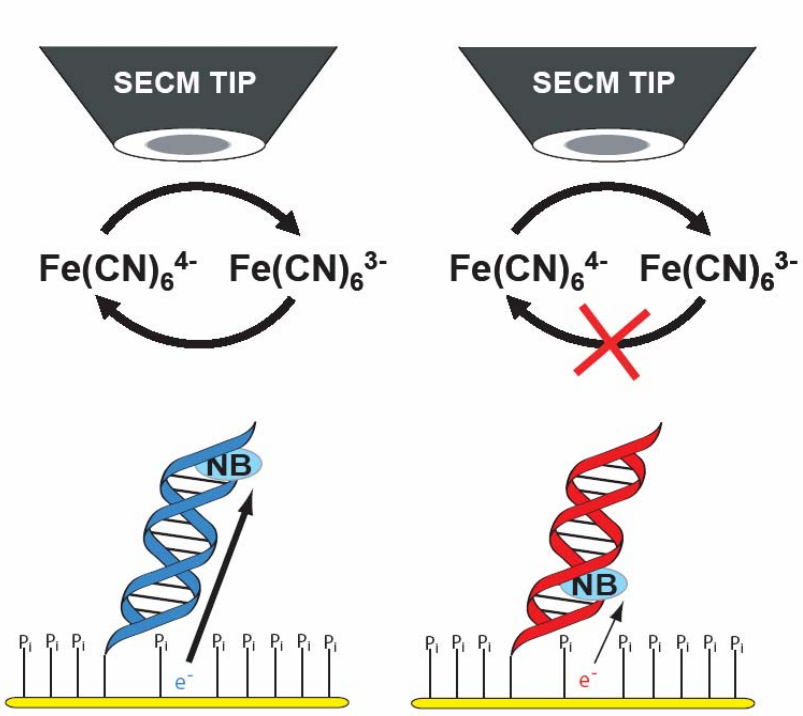

Figure 8.2: Schematic illustration of SECM imaging of DNA monolayers modified with Nile Blue (NB) at the top or the bottom; the negatively charged backfilling underlayer is also shown. The sequence was 5'-*U*GC GTG CTT TAT ATC TC-3' (top NB) and 5'-TGC GTG CTT TAT ATC *U*C-3' (bottom NB) where the italicized U indicates the location of the NB moiety.

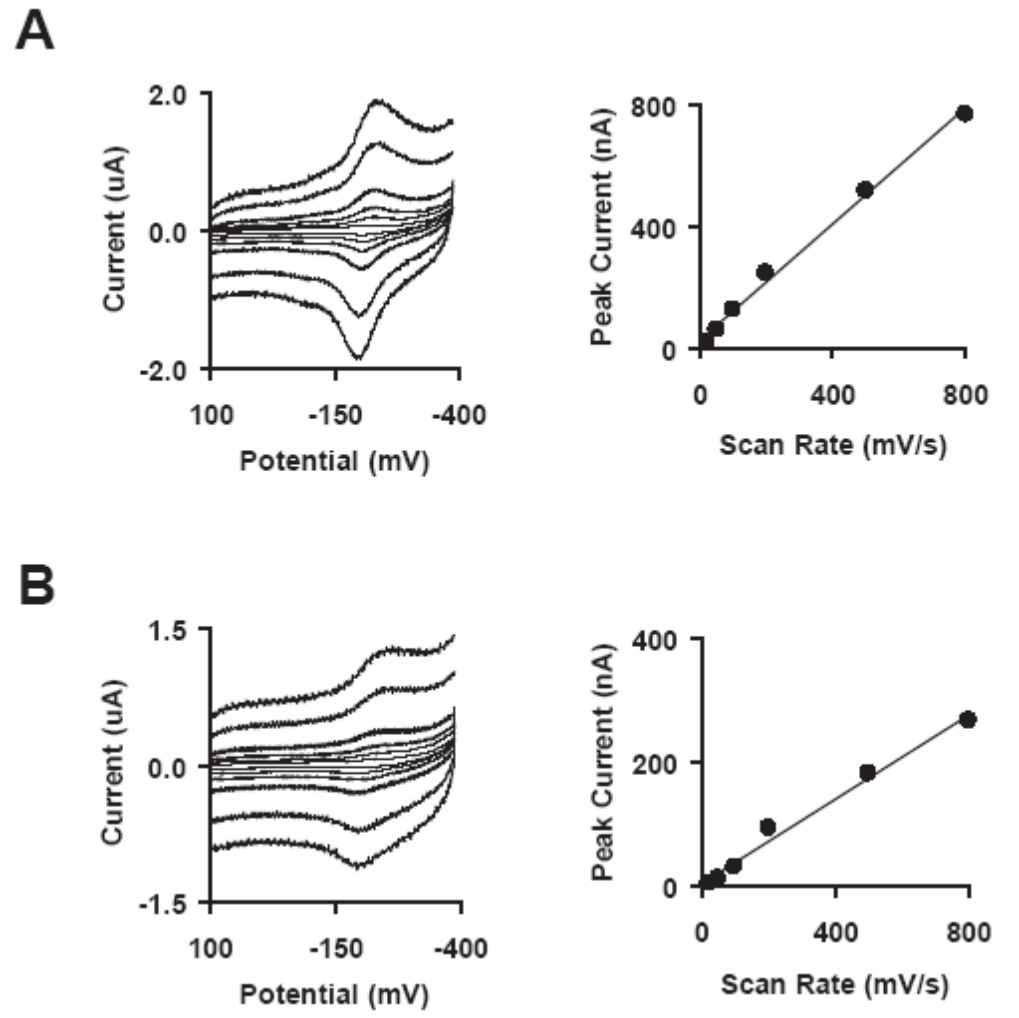

Figure 8.3: Cyclic voltammetry of DNA monolayers at various scan rates modified with NB at the bottom (A) and top (B) in pH =7.1, 5 mM NaPi, 50 mM NaCl buffer. The corresponding plots of peak current as a function of scan rate are shown on the right. The sequence was 5'-TGC GTG CTT TAT ATC *U*C-3' (bottom NB) and 5'-*U*GC GTG CTT TAT ATC TC-3' (top NB) where the italicized U indicates the location of the NB moiety.

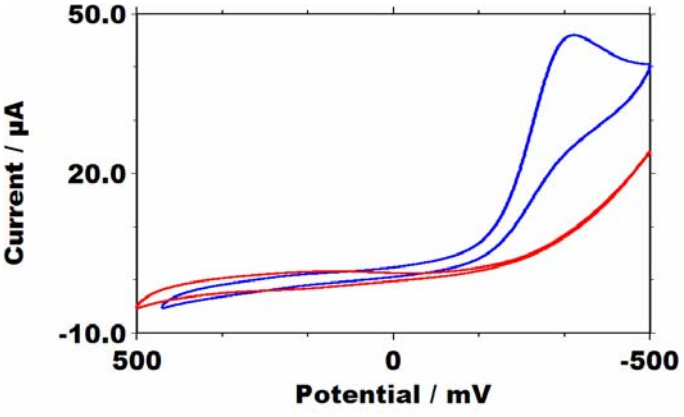

Figure 8.4: Cyclic voltammetry at 100 mV/s of DNA monolayers modified with NB at the top (blue) and bottom (red) in 80 mM NaCl, 20 mM NaP_i, pH= 7.2, 5 mM $K_3Fe(CN)_6$ buffer. The sequence was 5'-*U*GC GTG CTT TAT ATC TC-3' (top NB) and 5'-TGC GTG CTT TAT ATC *U*C-3' (bottom NB) where the italicized U indicates the location of the NB moiety. Note that a catalytic peak is only observed for a DNA monolayer modified with NB at the top.

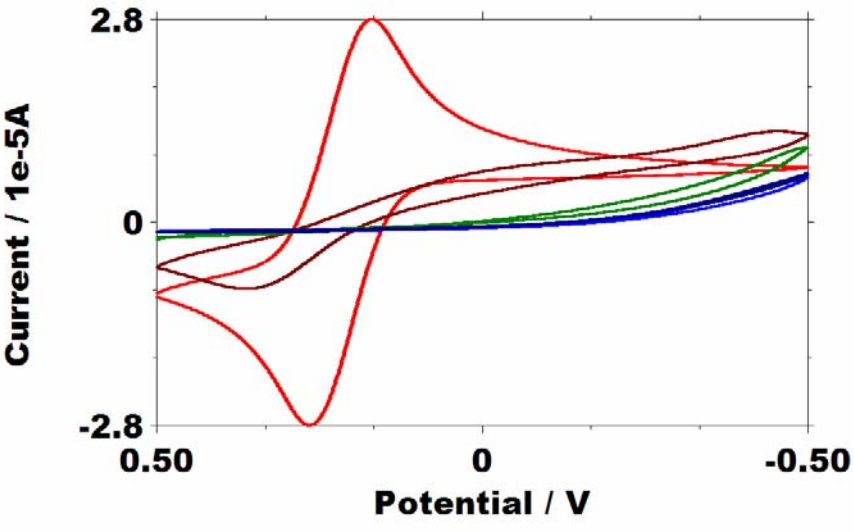

Figure 8.5: Successive cyclic voltammograms of ferricyanide at a bare Au electrode in pH =7.1, 5 mM NaPi, 50 mM NaCl buffer before (red) and after (other colors) addition of 1 mM 11-mercaptoundecylphosphoric acid to the buffer. The voltammograms correspond to different exposure times in the 11-mercaptoundecylphoshoric acid containing buffer. Complete attenuation of the ferricyanide signal is observed within 15 minutes.

The DNA monolayers were backfilled with 11-mercaptoundecylphoshoric acid, a negatively charged alkanethiol which completely passivates against ferricyanide (Figure 8.4 and Figure 8.5). Importantly, the presence of this underlayer makes it more likely that the DNA is electrostatically repelled by the negatively charged surface (47), ensuring an upright orientation in a dilute film. For a DNA monolayer modified with NB at the top, only an asymmetric cathodic peak is observed at the reduction potential of NB. However, for a DNA monolayer modified with NB at the bottom, the catalytic peak is absent. This data strongly indicates that only solution-exposed NB is capable of reducing ferricyanide.

8.3.2 SECM of DNA Monolayers Modified with Nile Blue in Feedback Mode

To visualize the NB/ferricyanide catalytic cycle both locally and directly (8, 46), we carried out SECM measurements at DNA monolayers covalently modified with NB (Figure 8.1). In these experiments, $Fe(CN)_6^{4-}$ is oxidized in solution at a platinum SECM tip, yielding a steady-state, diffusion-controlled current. The SECM tip is then physically lowered toward the DNA-modified gold substrate at a constant rate, and the current-distance feedback curve is recorded at various substrate bias potentials. If reduction of tip-generated $Fe(CN)_6^{3-}$ at the underlying substrate is blocked by the monolayer, the steady-state tip current drops upon approach (negative feedback) due to restricted diffusion of bulk ferrocyanide. If, on the other hand, the rate of catalytic $Fe(CN)_6^{3-}$ reduction *via* reduced NB at the modified substrate is rapid, redox cycling between the tip and substrate occurs, yielding increased tip currents (positive feedback).

As shown in Figure 8.6, films containing NB attached at the bottom of the DNA helices result in complete negative feedback at substrate bias potentials of both 0 mV and -400 mV. At 0 mV, bound NB remains in its oxidized state and there is a relatively small

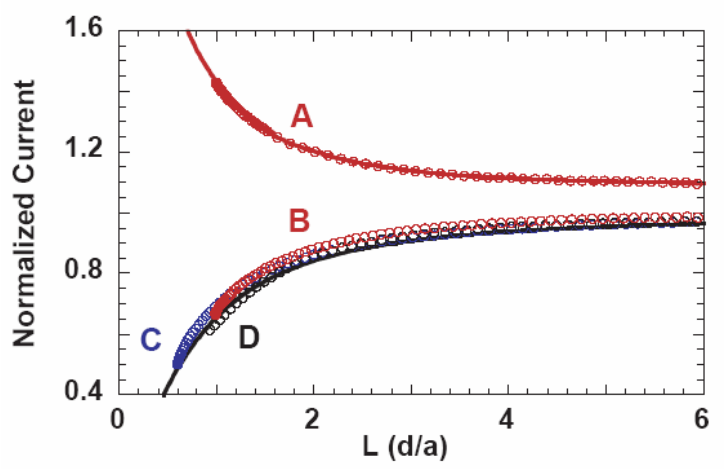

Figure 8.6: SECM approach curves obtained for DNA monolayers modified with NB at the top and bottom in 80 mM NaCl, 20 mM NaP_i, pH= 7.2, 5 mM $K_4Fe(CN)_6$ buffer with a tip-approach speed of 1 μm/s. The tip approach current has been normalized by the tip steady-state current at an infinite distance from the substrate. The normalized current is plotted against d/a where d is the tip/substrate separation and a represents the tip radius. For the DNA monolayer functionalized with NB at the top, positive feedback is observed at -400 mV (**A**), and negative feedback is observed at 0 mV (**B**). For the DNA monolayer modified with NB at the bottom, negative feedback is observed both at 0 mV (**C**) and -400 mV (**D**). Theoretical curves are shown for ideal negative feedback at an insulating substrate (black solid line) and for finite heterogeneous kinetics with a rate constant of k_{app}=4.6*10^{-2} cm/s for this specific substrate (red solid line).

(~ 200 mV) overpotential for ferricyanide reduction. At -400 mV, however, the NB is fully reduced and the substrate overpotential increases to ~ 600 mV. Despite this high driving force and the ability of reduced NB to act as a redox catalyst, the SECM response mimics that expected for a purely insulating substrate. This indicates sufficient electrostatic repulsion at the DNA/phosphate-terminated surface to effectively block tip-generated ferricyanide not only from the underlying gold electrode (26, 28) but also from the reduced NB buried deep within the DNA film.

A markedly different response is observed for DNA monolayers modified with NB at the top of the film. At substrate bias potentials of 0 mV, pure negative feedback is again observed. However, when the substrate bias voltage is held at -400 mV (a value negative of the formal reduction potential of NB) the response switches to positive feedback. Such a response signals rapid CT between tip-generated $Fe(CN)_6^{3-}$ and reduced NB, which is now bound at the solvent-exposed periphery of the monolayer. Indeed, assuming that the tip current is controlled by NB-mediated CT through the DNA film, the approach curve can be modeled using well-known analytical approximations for finite heterogeneous kinetics (53–55). The fits in Figure 8.6 show excellent agreement with the approximations both for the insulating monolayers (black solid line for negative feedback) and for the finite heterogeneous kinetics of ferricyanide reduction (red solid line for positive feedback). The one-parameter fit shown in Figure 8.6A for the DNA film modified at the top corresponds to a surprisingly rapid apparent rate constant for regeneration of ferricyanide of $k_{app}= 6 \pm 3 * 10^{-2}$ cm/s as measured at -400 mV versus SSCE (over four independent trials).

Two pieces of experimental evidence further substantiate the proposed DNA-mediated pathway for the SECM response. First, DNA quantification by ruthenium hexammine assay (56–58) for DNA films modified with NB either at the top or bottom yields very similar surface coverages (a minor contribution to the ruthenium hexammine signal is expected from 11-mercaptoundecylphosphoric acid due to its single phosphate group). Although this assay provides only a qualitative measure of surface coverage (58), it indicates nevertheless that both electrodes are covered with similar amounts of negative charge. Thus, for substrate potentials of -400 mV, the large discrepancy in ET rate across DNA films modified with NB at the top versus that modified at the bottom cannot be ascribed to relative differences in electrostatic screening of ferricyanide.

Second, DNA films modified with NB at the bottom can support electrocatalytic reduction of ferricyanide, but only upon addition of a redox mediator that has access to the film/solution interface. Thus, as an additional control experiment, the approach curve in SECM feedback mode was recorded for DNA monolayers modified with NB at the bottom before and after addition of 1.5 μM Methylene Blue (MB) to the solution (Figure 8.7). While the addition of MB does not change the observed negative feedback at a substrate potential of 0 mV, measurable positive feedback is found at substrate potentials negative of the MB redox couple. Analogous behavior was recently observed by Zhou for DNA-modified electrodes in the presence of MB in solution (28). The positive feedback observed in our experiments with MB is notably weaker *versus* that found for the monolayers covalently modified with NB at the top, and yields an apparent rate constant for ferricyanide reduction by non-covalent MB of $k_{app}=4.8 * 10^{-3}$ cm/s as measured at -300 mV versus SSCE, which is similar to that found earlier (28).

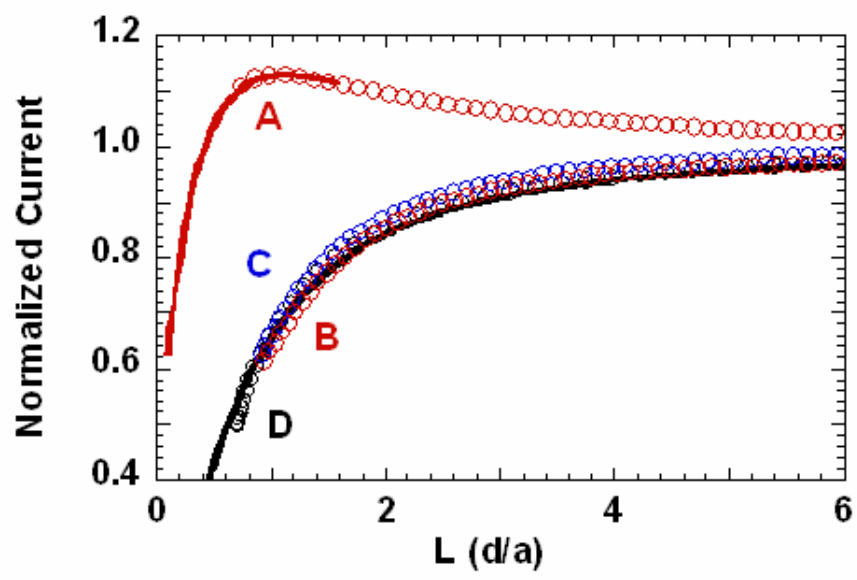

Figure 8.7: SECM approach curves taken for Nile Blue-DNA monolayers before (**C, D**) and after (**A, B**) addition of 1.5 μM Methylene Blue at substrate biases of 0 mV (**B, D**) and -300 mV (**A, C**). Approach curves were taken in pH= 7.2, 20 mM Na_2HPO_4, 80 mM NaCl, and 5 mM $K_4Fe(CN)_6$ buffer. The sequence was 5'-*U*GC GTG CTT TAT ATC TC-3' where the italicized U indicates the location of the NB moiety. Theoretical fits for finite heterogeneous kinetics with $k_{app}=4.8*10^{-3}$ cm/s and negative feedback are shown as solid lines for comparison.

Moreover, the MB controls yield essentially identical results with and without backfilling, revealing that MB cannot be simply incorporated within the 11-mercaptoundecylphosphoric acid underlayer. This experiment indicates that the DNA film modified with NB at the bottom supports long-range DNA-mediated CT, but measurable CT occurs only as long as the $Fe(CN)_6^{3-}$ in solution has access to the redox-active intercalator within the film.

8.3.3 SECM Imaging of DNA Monolayer Morphology

Previously, undiluted DNA monolayers of the type utilized during the course of this study have been characterized by atomic-force microscopy (22–24), fluorescence spectroscopy (59–61), surface-plasmon resonance (62), and radio-active tagging (12, 63). These experiments (along with electrochemical measurements) confirm that dense DNA films adopt an upright orientation with respect to the surface. However, a distinct geometric orientation of a dilute submonolayer film has been difficult to characterize conclusively with such techniques. To gain further insight into the morphology of DNA monolayers modified with NB, SECM in imaging mode was utilized to examine the DNA films. In general, the images indicate that the backfilled monolayers investigated here are electrostatically smooth within the one micron resolution of the SECM tip. The analysis of a large collection of images (hundreds collected over numerous substrates) indicates that some electrodes are completely and uniformly covered by the DNA film. On the other hand, some images feature domains on the electrode surface that are either DNA-free or contain thinner and less organized DNA assemblies. Indeed, such partially covered or imperfect DNA monolayers were found to correlate well with incomplete

passivation of ferricyanide at the substrate, allowing for a detailed analysis of even these imperfect surfaces with SECM.

Figure 8.8 shows images obtained for DNA substrates modified with NB at the top or bottom over an 85 μm by 85 μm scan area. The entire image is essentially flat and uniform with the exception of the small area in the rear corner, which was generated by close approach of the tip to the substrate upon initiation of the scan thereby resulting in a partially uncovered surface. Significantly, it is apparent that changing the substrate bias has only a small effect on the steady-state current at the tip for films functionalized with NB at the bottom, yielding nearly identical images at 0 mV and -400 mV. However, for the film functionalized with NB at the top, changing the substrate bias modulates or "switches" the entire area under the scan with a resulting significant enhancement of the steady-state current at -400 mV. These observations parallel those obtained via the feedback mode of the SECM and illustrate the powerful imaging capabilities of this technique.

Notably, the most efficient modulation occurs within regions of the DNA film that exhibit the lowest currents at substrate potentials of 0 mV (Figure 8.8A, 8.8B). This can be best illustrated by mapping the switching ratios i.e. the currents obtained at a substrate bias of -400 mV versus a substrate bias of 0 mV for both types of films (Figure 8.8C, 8.8D). For example, the DNA monolayer modified with NB at the top exhibits low currents at 0 mV over the entire scan area, except for the partially uncovered corner (rear corner in Figure 8.8A, 8.8C); at a substrate bias of -400 mV, the smallest current amplification is observed in this uncovered spot. On the other hand, the DNA monolayer

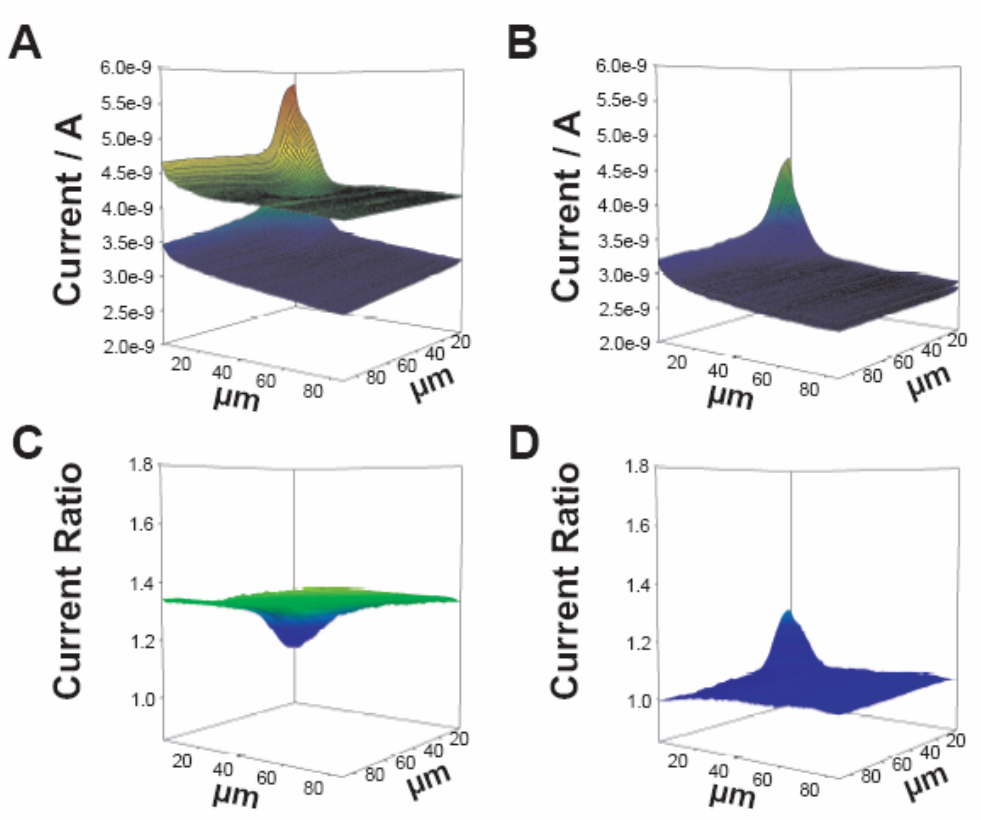

Figure 8.8: SECM images obtained for DNA monolayers modified with NB at the top (**A, C**) and NB at the bottom (**B, D**). The tip was polarized to 1 V, and the scans were performed in 80 mM NaCl, 20 mM NaP_i, pH= 7.2, 5 mM $K_4Fe(CN)_6$ buffer at a speed of 10 μm/s. The substrate bias was -400 mV (green in **A, B**) and 0 mV (blue in **A, B**). The switching ratios (the current obtained at -400 mV divided by the current obtained at 0 mV) are shown for monolayers with NB at the top (**C**) and monolayers with NB at the bottom (**D**). The poorly covered areas of the DNA monolayer are in the rear corners of **A**, **B**, **C**, and **D**.

\

modified with NB at the bottom exhibits low currents both at 0 mV and -400 mV over the well-covered areas of the scan. However, the poorly passivated region in the corner of the film with NB at the bottom (rear corner in Figure 8.8B, 8.8D) exhibits partial modulation when biased at -400 mV, hinting that the tip-generated $Fe(CN)_6^{3-}$ can access either some of the NB moieties or the bare gold surface. These observations demonstrate that the SECM allows for investigation of *imperfect* DNA films since it affords the ability to differentiate between catalytically active DNA spots and poorly passivated defects within the film.

8.3.4 Detection of TATA Binding Protein by SECM

As confirmation of the DNA-mediated nature of this cycle, approach curves were recorded at DNA monolayers featuring NB at the top before and after addition of TBP, a transcription factor which bends the DNA by ~ 90º thereby attenuating DNA CT upon binding (12, 13). Figure 8.9 shows a schematic illustration of the sequence-specific detection of TBP during an SECM experiment. As previously described, the tip is polarized at a potential sufficient for direct oxidation of $Fe(CN)_6^{4-}$ while the potential of the substrate is varied. Prior to addition of TBP, the ferricyanide/NB catalytic cycle is "turned on" at a substrate bias of -400 mV resulting in positive feedback (Figure 8.10A). Upon addition of TBP to a monolayer containing its binding site (5'-TATA-3'), the ferricyanide/NB catalytic cycle is "turned off" at a substrate bias of -400 mV resulting in negative feedback (Figure 8.10D). On the other hand, the feedback observed at DNA monolayers lacking the binding site is unaffected by the addition of TBP (Figure 8.10B, 10C). Therefore, the sequence-specific distortion of the DNA spacer by TBP inhibits the DNA-mediated electrochemistry of Nile Blue.

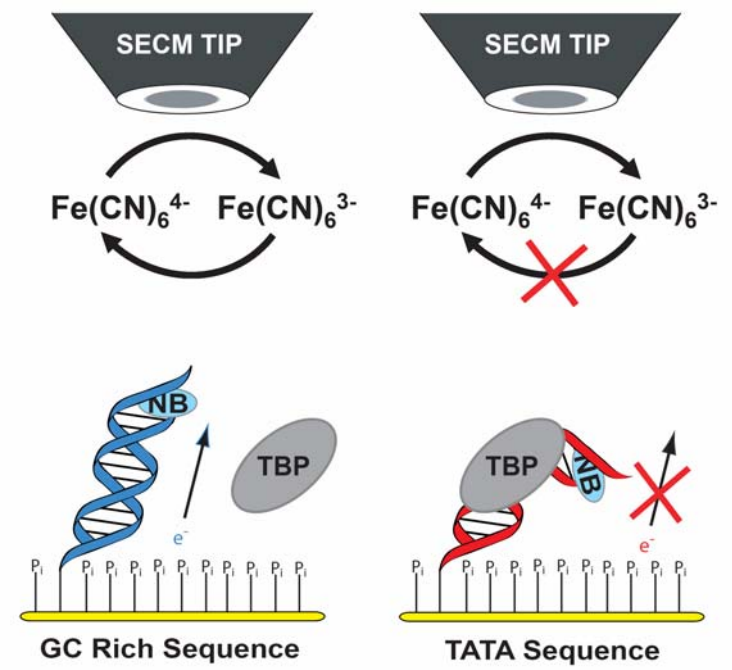

Figure 8.9: Schematic illustration of the SECM-based, sequence-specific detection of TBP binding at DNA monolayers modified with NB. The addition of TBP in the presence of its binding site (right) attenuates the NB/ferricyanide catalytic cycle. Without the binding site for TBP, no protein binding occurs and DNA-mediated CT proceeds.

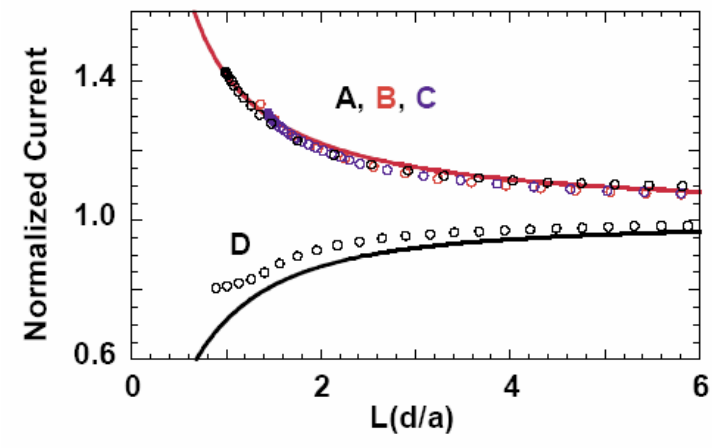

Figure 8.10: SECM approach curves taken for Nile Blue-DNA monolayers with (**A, D**) and without (**B, C**) the TBP binding site before (**A, B**) and after (**C, D**) addition of 100 nM TBP. Note that the addition of TBP eliminates the positive feedback observed at the DNA monolayer containing the 5'-TATA-3' binding site but has no effect on the other sequence. Approach curves were obtained in 20 mM Na_2HPO_4, 80 mM NaCl, and 5 mM $K_4Fe(CN)_6$, pH= 7.2, at an approach speed of 1 μm/s. The tip was polarized at 1 V with the substrate polarized at -400 mV. The sequences were 5'-*U*GC GTG CTT TAT ATC TC-3' and 5'-*U*GC GCG CCC GGC GCC TC-3' where the italicized U indicates the location of the NB moiety.

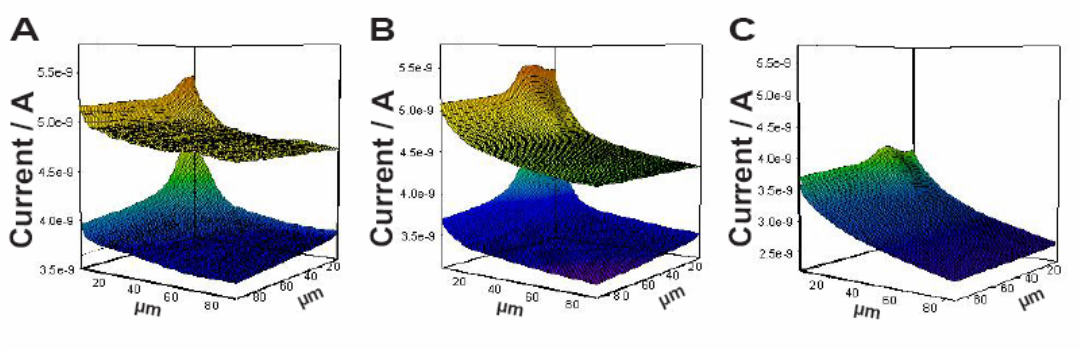

Figure 8.11: Scanning electrochemical microscopy images of a Nile Blue-DNA monolayer with a substrate bias of -400 mV (yellow) and 0 mV (blue). The tip was polarized at 1 V, and the scan rate was 10 μm/s. Images were obtained in pH= 7.2, 20 mM Na_2HPO_4, 80 mM NaCl, and 5 mM $K_4Fe(CN)_6$ buffer before protein addition (A), after addition of 1 μM BSA (B), and after addition of 300 nM TBP (C). After addition of TBP, the scans are identical regardless of substrate bias (the plots in C completely overlap).

To further explore the analytical capabilities of the SECM, TBP binding at DNA monolayers was also investigated in imaging mode (Figure 8.11). Before addition of protein, a ~ 30 % increase in the steady-state current is observed over nearly the entire 85 μm by 85 μm scan area upon modulation of the substrate potential from 0 mV to -400 mV (note that the partially uncovered area in the rear corner exhibits the poorest current modulation in Figure 8.11A). Upon addition of 1 μM BSA to the solution, the steady-state tip current is slightly lowered (Figure 8.11B). However, there is no effect on the switching behavior of the substrate with the degree of modulation remaining at ~ 30 %, and these observations are consistent with some non-specific adsorption of BSA at the tip and substrate (12). Subsequently, the addition of 300 nM TBP then further lowers the steady-state tip current, presumably through non-specific adsorption (Figure 8.11C), and importantly, this transcription factor eliminates "switching" over nearly the entire scan area, indicating reliable detection of TBP binding in a localized area of the monolayer.

These results provide strong support for the DNA-mediated nature of the Nile Blue/ferricyanide catalytic cycle. It is particularly striking that TBP binding eliminates positive feedback given that bending the DNA brings NB (and presumably ferricyanide) closer to the surface. In fact, upon binding, TBP should shield the negatively charged DNA and reduce the electrostatic repulsion of ferricyanide from the negatively charged monolayer. If significant direct charge transfer between the surface and tip generated ferricyanide were occurring (as observed by Bard and coworkers) (26), there would be an enhancement in the tip current at -400 mV upon addition of TBP, yet the opposite effect is observed here.

8.4 Discussion

We have now utilized the SECM to demonstrate electrocatalytic signal amplification at DNA monolayers modified with NB. Positive feedback was observed for DNA monolayers modified with NB at the top and the substrate biased at potentials sufficiently negative to reduce NB. However, only negative feedback was observed for DNA monolayers modified with NB at the bottom, regardless of the substrate bias. These measurements have allowed us to extract an apparent heterogeneous rate constant for ferricyanide reduction by DNA-bound NB of $k_{app}= 6 \pm 3*10^{-2}$ cm/s, indicating that such probe-modified DNA monolayers may behave somewhat like conducting films (26). Furthermore, we have shown the sequence-specific interruption of the ferricyanide/NB electrocatalytic cycle upon addition of the TBP transcription factor: positive feedback is completely eliminated upon addition of this protein. Taken together, these data strongly indicate that the redox chemistry of NB is DNA-mediated.

Previous studies (22, 24, 59, 60) have indicated that the individual duplexes within dense DNA SAMs stand upright at potentials negative of the PZC, particularly in the presence of an alkanethiol underlayer (61, 62). These findings were hinted by our observations for the electrochemistry of MB at dense DNA monolayers, where only the MB constrained to the periphery of the film was available for the MB/ferricyanide catalytic cycle (8, 46). The present results for sparse films are fully consistent with an upright orientation of the DNA. By fixing the location of the NB covalent probe, we have conclusively demonstrated that only those monolayers which feature NB at the top of the

film and close to the film/solution interface can mediate catalytic ferrocyanide recycling at the probe tip.

The images obtained over micron areas of DNA monolayers modified with NB are consistent with the approach curves in feedback mode. Notably, the imaging mode of the SECM allows for the reliable investigation of imperfect DNA monolayers in multiple areas of the substrate, making it an attractive complement to bulk voltammetric techniques. In addition, the SECM can distinguish between areas with and without DNA by carefully monitoring the ratio of the currents at various substrate biases. Therefore, unlike substrate voltammetry, the SECM ensures that the observed electrochemical response is due solely to DNA-mediated electrochemistry. This feature of SECM allows for the highly reliable detection of protein binding, minimizing the possibility of false positives that can arise in experiments involving only substrate voltammetry.

As a surface characterization technique, the SECM also provides important information which is intermediate between centimeter scale electrochemical measurements and nanometer scale AFM/STM measurements. For example, an SECM tip with a 10 μm footprint will access attomoles of DNA molecules (for uniform surface coverages of 1–3 pmol/cm^2), thereby simultaneously sampling a large number of molecules (relative to an AFM/STM) and avoiding overwhelming contributions from defects in the monolayer (relative to substrate electrochemistry). In addition, assuming a 1:1 DNA/protein stoichiometry, we are consequently able to detect attomole quantities of the TBP transcription factor with the SECM, underscoring the potential of this methodology for highly sensitive, sequence-specific detection. Therefore, the scale and sensitivity of the instrument makes the SECM inherently compatible with multiplexed

technologies such as DNA microarrays, indicating that it is a potential alternative to fluorescence-based microarray technologies.

Overall, these results indicate that the investigation of DNA-mediated electrochemistry with scanning electrochemical microscopy is a powerful and flexible methodology for the localized investigation of DNA monolayers. Here, by backfilling with a negatively charged alkanethiol and coupling NB with ferricyanide in a catalytic cycle, we have ensured that the DNA duplexes adopt an upright orientation and that DNA CT dominates the electrochemical response observed by SECM. In fact, if non-specific protein adsorption at the tip can be minimized, the micron size and reliability of the SECM could lead to sensitive monitoring of DNA/protein interactions in a multiplexed format.

REFERENCES

(1) Boon, E. M., Barton, J. K. (2002) *Curr. Opin. Struct. Biol. 12*, 320–329.

(2) Delaney, S., Barton, J. K. (2003) *J. Org. Chem. 68*, 6475–6483.

(3) O'Neill, M. A., Barton, J. K. (2005) *Charge Transfer in DNA: From Mechanism to Application* (H.-A. Wagenknecht), pp. 27–75, Wiley-VCH, Hoboken.

(4) Giese, B. (2000) *Acc. Chem. Res. 33*, 631–636.

(5) Schuster, G. B. (2000) *Acc. Chem. Res. 33*, 253–260.

(6) Drummond, T. G., Hill, M. G., Barton, J. K. (2003) *Nature Biotechnol. 21*, 1192–1199.

(7) Odenthal, K. J., Gooding, J. J. (2007) *Analyst 132*, 603–610.

(8) Kelley, S. O., Boon, E. M., Barton, J. K., Jackson, N. M., Hill, M. G. (1999) *Nucleic Acids Res. 27*, 4830–4837.

(9) Boon, E. M., Ceres, D. M., Drummond, T. G., Hill, M. G., Barton, J. K. (2000) *Nature Biotechnol. 18*, 1096–1100.

(10) Gorodetsky, A. A., Barton, J. K. (2006) *Langmuir 22*, 7917–7922.

(11) Boal, A. K., Barton, J. K. (2005) *Bioconjugate Chem. 16*, 312–321.

(12) Boon, E. M., Salas, J. E., Barton, J. K. (2002) *Nature Biotechnol. 20*, 282–286.

(13) Gorodetsky, A. A., Ebrahim, A., Barton, J. K. (2008) *J. Am. Chem. Soc. 130*, 2924–2925.

(14) Boon, E. M., Livingston, A. L., Chmiel, N. H., David, S. S., Barton, J. K. (2003) *Proc. Natl. Acad. Sci. U. S. A. 100*, 12543–12547.

(15) Boal, A. K., Yavin, E., Lukianova, O. A., O'Shea, V. L., David, S. S., Barton, J. K. (2005) *Biochemistry 44*, 8397–8407.

(16) Gorodetsky, A. A., Boal, A. K., Barton, J. K. (2006) *J. Am. Chem. Soc. 128*, 12082–12083.

(17) DeRosa, M. C., Sancar, A., Barton, J. K. (2005) *Proc. Natl. Acad. Sci. U. S. A. 102,* 10788–10792.

(18) Gorodetsky, A. A., Dietrich, L. E. P., Lee, P. E., Demple, B., Newman, D. K., Barton, J. K. (2008) *Proc. Natl. Acad. Sci. U. S. A. 105,* 3684–3689.

(19) D. M. Ceres, J. K. Barton. (2003) *J. Am. Chem. Soc. 125*, 14964–14965.

(20) Hihath, J., Xu, B., Zhang, P., Tao, N. (2005) *Proc. Natl. Acad. Sci. U. S. A. 102,* 16979–16983.

(21) Wierzbinski, E., Arndt, J., Hammond, W., Slowinski, K. (2006) *Langmuir 22,* 2426–2429.

(22) Kelley, S. O., Barton, J. K., Jackson, N. M., McPherson, L. D., Potter, A. B., Spain, E. M., Allen, M. J., Hill, M. G. (1998) *Langmuir 14*, 6781–6784.

(23) Zhou, D., Sinniah, K., Abell, C., Rayment, T. (2002) *Langmuir 18*, 8278–8281.

(24) Erts, D., Polyakov, B., Olin, H., Tuite, E. (2003) *J. Phys. Chem. B. 107*, 3591–3597.

(25) Turcu, F., Schulte, A., Hartwich, G., Schuhmann, W. (2004) *Angew. Chem. Int. Ed. 43*, 3482–3485.

(26) Liu, B., Li, C.-Z., Kraatz, H.-B., Bard, A. J. (2005) *J. Phys. Chem. B. 109*, 5193–5198.

(27) Wang, K., Goyer, C., Anne, A., Demaille, C. (2007) *J. Phys. Chem. B. 111,* 6051–6058.

(28) Wain, A. J., Zhou, F. (2008) *Langmuir 24,* 5155–5160.

(29) Stoica, L., Neugebauer, S., Schuhmann, W. (2008) *Adv. Biochem. Eng. Biot. 109*, 455–492.

(30) Bard, A. J., Mirkin, M. V., eds. (2001) *Scanning Electrochemical Microscopy*, Marcel Dekker: New York.

(31) Wang, J., Zhou, F. (2002) *J. Electroanal. Chem. 537*, 95–102.

(32) Komatsu, M., Yamashita, K., Uchida, K., Kondo, H., Takenaka, S. (2006) *Electrochim. Acta 51*, 2023–2029.

(33) Lie, L. H., Mirkin, M. V., Hakkarainen, S., Houlten, A., Horrocks, B. R. (2007) *J. Electroanal. Chem. 603*, 67–80.

(34) Palchetti, I., Laschi, S., Marrazza, G., Mascini, M. (2007) *Anal. Chem. 79*, 7206–7213.

(35) Wong, E. L. S., Gooding, J. J. (2006) *Anal. Chem. 78*, 2138–2144.

(36) Li, X., Song, H., Nakatani, K., Kraatz, H.-B. (2007) *Anal. Chem. 79,* 2552–2555.

(37) Wong, E. L. S., Gooding, J. J. (2007) *J. Am. Chem. Soc. 129*, 8950–8951.

(38) Di Giusto, D. A., Wlasoff, W. A., Giesebrecht, S., Gooding, J. J., King, G. C. (2004) *J. Am. Chem. Soc. 126*, 4120–4121.

(39) Kelley, S. O., Jackson, N. M., Hill, M. G., Barton, J. K. (1999) *Angew. Chem., Int. Ed. 38*, 941–945.

(40) Drummond, T. G., Hill, M. G., Barton, J. K. (2004) *J. Am. Chem. Soc. 126*, 15010–15011.

(41) Liu, T., Barton, J. K. (2005) *J. Am. Chem. Soc. 127*, 10160–10161.

(42) Gorodetsky, A. A., Green, O., Yavin, E., Barton, J. K. (2007) *Bioconjugate Chem. 18*, 1434–1441.

(43) Okamoto, A., Kamei, T., Tanaka, K., Saito, I. (2004) *J. Am. Chem. Soc. 126*, 14732–14733.

(44) Okamoto, A., Kamei, T., Saito, I. (2006) *J. Am. Chem. Soc. 128*, 658–662.

(45) Inouye, M., Ikeda, R., Takase, M., Tsuri, T., Chiba, J. (2005) *Proc. Natl. Acad. Sci. U. S. A. 102*, 11606–11610.

(46) Boon, E. M., Barton, J. K., Bhagat, V., Nersissian, M., Wang, W., Hill, M. G. (2003) *Langmuir 19*, 9255–9259.

(47) Zhang, J., Kirkham, J., Robinson, C., Wallwork, M. L., Smith, D. A., Marsh, A., Wong, M. (2000) *Anal. Chem. 72*, 1973–1978.

(48) Liu, H.-H., Lu, J.-L., Zhang, M., Pang, D.-W. (2002) *Anal. Sci. 18*, 1339–1344.

(49) Ju, H., Ye, Y., Zhu, Y. (2005) *Electrochim. Acta 50*, 1361–1367.

(50) Schlereth, D. D., Schmidt, H.-L. (1995) *J. Electroanal. Chem. 380*, 117–125.

(51) Sugawara, K., Yamauchi, Y., Hoshi, S., Akatsuka, K., Yamamoto, F., Tanaka, S., Nakamura, H. (1996) *Bioelectrochem. Bioenerg. 41,* 167–172.

(52) Bard, A. J., Faulkner, L. R. (2001) *Electrochemical Methods*, *2nd ed.*, John Wiley & Sons: New York.

(53) Mirkin, M.V., Arca, M., Bard, A. J. (1993) *J. Phys. Chem. 97*, 10790–10795.

(54) Wei, C., Bard, A.J., Mirkin, M.V. (1995) *J. Phys. Chem. 99*, 16033–16042.

(55) Lefrou, C. (2007) *J. Electroanal. Chem. 601*, 94–100.

(56) Steel, A. B., Herne, T. M., Tarlov, M. J. (1998) *Anal. Chem. 70*, 4670–4677.

(57) Yu, H.-Z., Luo, C.-Y., Sankar, D. G., Sen, D. (2003) *Anal. Chem. 75*, 3902–3907.

(58) Ceres, D. M., Udit, A. K., Hill, H. D., Hill, M. G., Barton, J. K. (2007) *J. Phys. Chem. B. 111*, 663–668.

(59) Rant, U., Arinaga, K., Fujita, S., Yokoyama, N., Abstreiter, G., Tornow, M. (2004) *Nano Lett. 4*, 2441–2445.

(60) Rant, U., Arinaga, K., Fujita, S., Yokoyama, N., Abstreiter, G., Tornow, M. (2004) *Langmuir 20*, 10086–10092.

(61) Arinaga, K., Rant, U., Tornow, M., Fujita, S., Abstreiter, G., Yokoyama, N. (2006) *Langmuir 22*, 5560–5562.

(62) Yang, X., Wang, Q., Wang, K., Tan, W., Yao, J., Li, H. (2006) *Langmuir 22*, 5654–5659.

(63) Gore, M. R., Szalai, V. A., Ropp, P. A., Yang, I. V., Silverman, J. S., Thorp, H. H. (2003) *Anal. Chem. 75*, 6586–6592.